

Camera-Aware Multi-Resolution Analysis for Raw Sensor Data Compression

Yeejin Lee, *Student Member, IEEE*, Keigo Hirakawa, *Senior Member, IEEE*, and Truong Q. Nguyen, *Fellow, IEEE*

Abstract—We propose a novel lossless and lossy compression scheme for color filter array (CFA) sampled images based on the wavelet transform of them. Our analysis suggests that the wavelet coefficients of *HL* and *LH* subbands are highly correlated. Hence, we decorrelate Mallat wavelet packet decomposition to further sparsify the coefficients. In addition, we develop a camera processing pipeline for compressing CFA sampled images aimed at maximizing the quality of the color images constructed from the compressed CFA sampled images. We validated our theoretical analysis and the performance of the proposed compression scheme using images of natural scenes captured in a raw format. The experimental results verify that our proposed method improves coding efficiency relative to the standard and the state-of-the-art compression schemes CFA sampled images.

Index Terms—Color filter array, image compression, camera processing pipeline, wavelet transform, JPEG.

I. INTRODUCTION

COLOR filter array (CFA) refers to a spatial multiplexing of red, green, and blue filters over the image sensor surface. The popular Bayer CFA pattern is shown in Fig. 1. The raw sensor data captured by this configuration is therefore a subsampled version of a full-color image, where each pixel sensor measures the intensity of only a red, green, or blue value. Demosaicking process interpolates the raw image and recovers the full-color image representation. Besides demosaicking, the captured data undergo defective sensor pixel removal, color correction, gamma correction, noise suppression, etc. Once the camera processing pipeline renders the color image, an image compression algorithm transforms the processed image to a storage format that requires fewer bits.

When compressing the image data, a digital data representation of the best quality is highly desirable in many applications, such as digital cinema, broadcast, medical imaging, image archives, etc. In such applications, lossless compression is preferable so that the original data can be reconstructed perfectly. However, lossless compression often requires large storage space. Hence, lossy compression, which could significantly reduce data size for storing, processing, and transmitting, is more common in consumer applications.

On the other hand, photographers often work directly with raw sensor data to maximize control over the post-processing. However, storing raw sensor data is difficult. With no standard method for compressing this type of data, the storage size

Y. Lee and T. Q. Nguyen are with the Department of Electrical and Computer Engineering, University of California, San Diego, CA, 92093 USA (e-mail: yel031@eng.ucsd.edu, tqn001@eng.ucsd.edu).

K. Hirakawa is with the Department of Electrical and Computer Engineering, University of Dayton, OH, 45469 USA (e-mail: khirakawa1@udayton.edu).

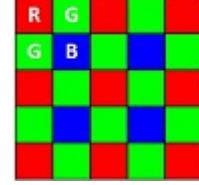


Fig. 1. Bayer color filter array pattern [16].

of the raw sensor data is typically very large. At the same time, compressing the raw sensor data also has the potential to improve compression performance relative to working with a full-color image. Despite the fact that the color images requires more bits to encode all color components, compression of CFA sampled images has received very limited attention in the literature [1–11].

To this end, we propose a novel compression scheme for raw sensor data. Our work is inspired by the CFA compression method of [9], the wavelet sampling theory of [12], and the demosaicking work of [13], [14]. Specifically, the CFA sampled image compression scheme in [9] leveraged a heuristic observation made about the behavior of the Mallat wavelet packet transform coefficients corresponding to the CFA sampled image. A more rigorous analysis of wavelet sampling in [12] revealed that Mallat wavelet coefficients are highly redundant. We previously used this fact to develop demosaicking [13], [14] and denoising methods [14].

The remainder of this article is organized as follows. In Section II, we provide theoretical analysis and review of wavelet transform for CFA sampled images. In Section III, we develop a scheme to further decorrelate the Mallat coefficients. We then propose a lossless and lossy compression of CFA sampled images leveraging this decorrelated Mallat wavelet structure. In addition, we design a camera processing pipeline aimed at maximizing the quality of the color images constructed from the compressed CFA sampled images. In Section IV, we verify the proposed scheme developed in Section III using real raw image sensor data. The preliminary results of this work appeared in [15].

II. BACKGROUND AND REVIEW

A. CFA Sampling

Let $\mathbf{x}(\mathbf{n}) = [r(\mathbf{n}) \ g(\mathbf{n}) \ b(\mathbf{n})]^T$ be a color image at the pixel location $\mathbf{n} = [n_0 \ n_1]$, where $r(\mathbf{n})$, $g(\mathbf{n})$, and $b(\mathbf{n})$ are the corresponding color tristimulus values of the color. Then the CFA sampled image $y(\mathbf{n}) : \mathbb{Z}^2 \rightarrow \mathbb{R}$ is

$$y(\mathbf{n}) = \mathbf{c}(\mathbf{n})\mathbf{x}(\mathbf{n}), \quad (1)$$

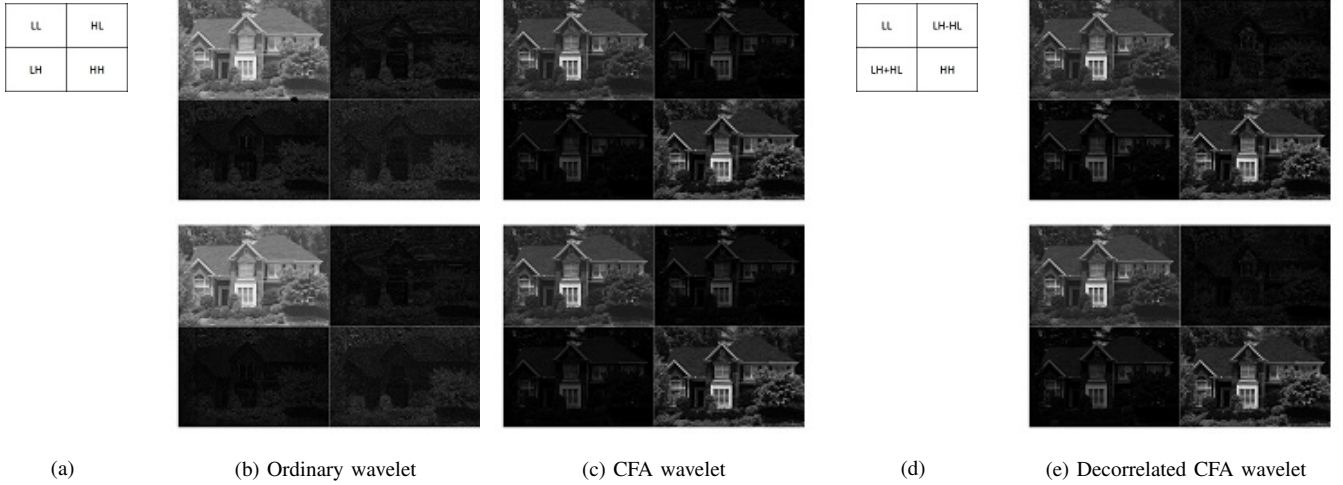


Fig. 2. The one-level (top row) LeGall 5/3 and (bottom row) Daubechies 9/7 wavelet transforms. (b) Wavelet coefficients of a typical grayscale image. (c) Wavelet coefficients of a CFA sampled image. (e) Wavelet coefficients of a CFA sampled image with the proposed decorrelation. The subband layout for (b) and (c) is shown in (a); the layout for (e) is shown in (d). Note that the coefficient magnitudes are scaled for display.

where $\mathbf{c} = [c_r(\mathbf{n}) \ c_g(\mathbf{n}) \ c_b(\mathbf{n})] : \mathbb{Z}^2 \rightarrow \{0, 1\}^3$ is a sampling indicator (e.g. $\mathbf{c}(\mathbf{n}) = [1 \ 0 \ 0]$ denotes a red sample at a pixel location \mathbf{n}).

Consider the Bayer pattern shown in Fig. 1. The CFA sampled image of (1) is rewritten as

$$\begin{aligned} \mathbf{y}(\mathbf{n}) &= \mathbf{c}(\mathbf{n}) \begin{bmatrix} 1 & 2 & 1 \\ 1 & 0 & -1 \\ 1 & -2 & 1 \end{bmatrix} \begin{bmatrix} \frac{1}{4} & \frac{1}{2} & \frac{1}{4} \\ \frac{1}{4} & 0 & -\frac{1}{4} \\ \frac{1}{4} & -\frac{1}{2} & \frac{1}{4} \end{bmatrix} \begin{bmatrix} r(\mathbf{n}) \\ g(\mathbf{n}) \\ b(\mathbf{n}) \end{bmatrix} \\ &= \mathbf{c}'(\mathbf{n}) \begin{bmatrix} \ell(\mathbf{n}) \\ \alpha(\mathbf{n}) \\ \beta(\mathbf{n}) \end{bmatrix}. \end{aligned} \quad (2)$$

Here, the luminance image $\ell(\mathbf{n})$ and the color difference images $\alpha(\mathbf{n})$ and $\beta(\mathbf{n})$ are defined as

$$\begin{aligned} \ell(\mathbf{n}) &:= \frac{1}{4}r(\mathbf{n}) + \frac{1}{2}g(\mathbf{n}) + \frac{1}{4}b(\mathbf{n}) \\ \alpha(\mathbf{n}) &:= \frac{1}{4}r(\mathbf{n}) - \frac{1}{4}b(\mathbf{n}) \\ \beta(\mathbf{n}) &:= \frac{1}{4}r(\mathbf{n}) - \frac{1}{2}g(\mathbf{n}) + \frac{1}{4}b(\mathbf{n}), \end{aligned} \quad (3)$$

where we interpret $\alpha(\mathbf{n})$, and $\beta(\mathbf{n})$ as proxies for two chrominance color components. This is convenient way to represent the CFA sampled image because $r(\mathbf{n})$, $g(\mathbf{n})$, and $b(\mathbf{n})$ share high spatial frequency components, yielding lowpass chrominance images $\alpha(\mathbf{n})$ and $\beta(\mathbf{n})$ [17], [18]. The modified CFA mask $\mathbf{d}(\mathbf{n})$ is defined as

$$\begin{aligned} \mathbf{c}'(\mathbf{n}) &= [d_\ell \ d_\alpha \ d_\beta] := \mathbf{c}(\mathbf{n}) \begin{bmatrix} 1 & 2 & 1 \\ 1 & 0 & -1 \\ 1 & -2 & 1 \end{bmatrix} \\ &= [1 \ (-1)^{n_1} + (-1)^{n_2} \ (-1)^{n_1+n_2}]. \end{aligned} \quad (4)$$

Hence, the CFA sampled data is rewritten as [13], [19], [20]

$$\mathbf{y}(\mathbf{n}) = \ell(\mathbf{n}) + d_\alpha(\mathbf{n})\alpha(\mathbf{n}) + d_\beta(\mathbf{n})\beta(\mathbf{n}). \quad (5)$$

In (5), the CFA sampled image is interpreted as a linear combination of a complete luminance component and highpass-modulated chrominance components.

B. Wavelet Transform of CFA Sampled Images

As observed in Fig. 2(c), it is empirically shown that the one-level wavelet transformation of a CFA sampled image is dominated by lowpass signals that are not sparse [9]. This observation is contradictory to the wavelet coefficients of ordinary color images in Fig. 2(b), where LH , HL , and HH subbands contain edges and details only. Consequently, the Mallat wavelet packet transform [21], [22] was proposed to further sparsify the detail coefficients of the CFA sampled images in HL , LH , and HH subbands.

A more rigorous analysis of the observation in [9] was provided in [12], which we briefly review below. Denote by w^y the first level wavelet decomposition of (5)

$$w_{i,j}^y(\mathbf{n}) = w_{i,j}^\ell(\mathbf{n}) + w_{i,j}^{d_\alpha \cdot \alpha}(\mathbf{n}) + w_{i,j}^{d_\beta \cdot \beta}(\mathbf{n}), \quad (6)$$

where the index $(i, j) \in \{L, H\}^2$ denotes the lowpass (L) and highpass (H) subbands in the vertical and horizontal directions, and w^ℓ corresponds to wavelet coefficients of the luminance image ℓ , etc [12], [18]. The wavelet transform of (6) is expanded as the combination of color difference image subbands, as follows:

$$\begin{aligned} w_{LL}^y(\mathbf{n}) &= w_{LL}^\ell(\mathbf{n}) + w_{LH^*}^\alpha(\mathbf{n}) + w_{H^*L}^\alpha(\mathbf{n}) + w_{H^*H^*}^\beta(\mathbf{n}) \\ w_{LH}^y(\mathbf{n}) &= w_{LH}^\ell(\mathbf{n}) + w_{L^*L}^\alpha(\mathbf{n}) + w_{H^*H}^\alpha(\mathbf{n}) + w_{H^*L^*}^\beta(\mathbf{n}) \\ w_{HL}^y(\mathbf{n}) &= w_{HL}^\ell(\mathbf{n}) + w_{L^*L}^\alpha(\mathbf{n}) + w_{HH^*}^\alpha(\mathbf{n}) + w_{L^*H^*}^\beta(\mathbf{n}) \\ w_{HH}^y(\mathbf{n}) &= w_{HH}^\ell(\mathbf{n}) + w_{L^*H}^\alpha(\mathbf{n}) + w_{HL^*}^\alpha(\mathbf{n}) + w_{L^*L^*}^\beta(\mathbf{n}), \end{aligned} \quad (7)$$

where L^* and H^* denote the subbands of conjugated wavelet transform coefficients computed using conjugated wavelet filters [12]. Owing to the lowpass nature of α and β , the wavelet

coefficients of w^α and w^β approximates to zero ($w_{LH}^\alpha \simeq 0$, $w_{HL}^\alpha \simeq 0$, etc.). Then, the wavelet analysis in [12] yields the following simplification of (7):

$$\begin{aligned} w_{LL}^y(\mathbf{n}) &\simeq w_{LL}^\ell(\mathbf{n}) \\ w_{LH}^y(\mathbf{n}) &\simeq w_{LH}^\ell(\mathbf{n}) + w_{L^*L}^\alpha(\mathbf{n}) \\ w_{HL}^y(\mathbf{n}) &\simeq w_{HL}^\ell(\mathbf{n}) + w_{L^*L}^\alpha(\mathbf{n}) \\ w_{HH}^y(\mathbf{n}) &\simeq w_{HH}^\ell(\mathbf{n}) + w_{L^*L}^\beta(\mathbf{n}). \end{aligned} \quad (8)$$

Hence, the wavelet coefficients w_{LH}^y , w_{HL}^y , and w_{HH}^y of a CFA sampled image in (8) are interpreted as sum of fine-scale luminance wavelet coefficients and chrominance conjugate scaling coefficients [13], [14]. Indeed, the wavelet coefficients of LH , HL , and HH subbands in Fig. 2(c) are dominated by lowpass signal of the chrominance images $w_{L^*L}^\alpha$ and $w_{L^*L}^\beta$, and $w_{L^*L}^\beta$.

C. Digital Camera Processing Pipeline

Digital camera processing pipeline refers to a sequence of image processing steps that are designed to recover a displayable image from the raw sensor data. We briefly review the basic steps taken, though there are variations among the camera manufacturers on the exact implementations. The steps we describe below are pertinent to the lossy compression algorithm we develop in Section III-D below.

Let $y(\mathbf{n})$ denote the raw image sensor data. We first subtract the so-called ‘‘black offset’’ $\mathbf{k} = [k_r \ k_g \ k_b]^T$, as follows:

$$y'(\mathbf{n}) = y(\mathbf{n}) - \mathbf{c}(\mathbf{n})\mathbf{k}. \quad (9)$$

This step is designed to map the digital values from the analog-to-digital converter (ADC) to a number that is linear to the light intensity so that a $y'(\mathbf{n})$ would map to zero when there is no light coming into the camera.

Following the black offset, the step known as ‘‘demosaicking’’ estimates the color image $\mathbf{x}(\mathbf{n})$ from the CFA sampled image $y'(\mathbf{n})$ [13], [14], [17–20]. In a step known as ‘‘color correction’’, the colors of the recovered image $\hat{\mathbf{x}}(\mathbf{n})$ corresponding to the spectral transmittance of the color filters are converted to a canonical color space by multiplying by a color transformation matrix $\mathbf{A} \in \mathbb{R}^{3 \times 3}$:

$$\mathbf{x}_{cc}(\mathbf{n}) = \mathbf{A}\hat{\mathbf{x}}(\mathbf{n}). \quad (10)$$

The ‘‘white balance’’ step rescales the color to make the color (nearly) invariant to illumination color [23–25],

$$\mathbf{x}_{wb,cc}(\mathbf{n}) = \begin{bmatrix} 1/i_r & 0 & 0 \\ 0 & 1/i_g & 0 \\ 0 & 0 & 1/i_b \end{bmatrix} \mathbf{x}_{cc}(\mathbf{n}). \quad (11)$$

where $[i_r, i_g, i_b]$ is the color of the illumination. Lastly, a compander known as gamma correction enhances the low-intensity pixels while compressing the high-intensity pixels by a non-linear mapping [26]. For example, gamma correction used in sRGB standard take the form [27]:

$$\mathbf{x}_{gc,wb,cc}(\mathbf{n}) = \begin{cases} 12.92\mathbf{x}_{wb,cc}(\mathbf{n}), & \text{if } \mathbf{x}_{wb,cc}(\mathbf{n}) \leq 0.0031308 \\ (1 + 0.055)\mathbf{x}_{wb,cc}(\mathbf{n})^{1/2.4} - 0.055, & \text{otherwise.} \end{cases} \quad (12)$$

Although other steps (e.g. defective pixel removal and noise suppression) are also common, black offset, demosaicking, color correction, white balance, and gamma correction are considered bare minimum steps. The processed color image $\mathbf{x}_{gc,wb,cc}(\mathbf{n})$ is considered the final output of the digital camera—it is either displayed or compressed and stored.

III. PROPOSED COMPRESSION SCHEME OF CFA SAMPLED IMAGE

The wavelet analysis in Section II-A and Section II-B suggests that the wavelet coefficients of a CFA sampled image are combinations of their luminance wavelet component and modulated frequency chrominance component. This implies that the LH , HL , and HH subbands directly yield poor coding efficiency, because $w_{L^*L}^\alpha$ and $w_{L^*L}^\beta$ would never achieve the coding efficiency of w_{LH}^y and w_{HL}^y even if further wavelet transform is applied. Hence, we instead propose to decorrelate LH and HL subbands based on the wavelet analysis in Section II.

In Section III-A, we develop a lossless compression method based on the decorrelated Mallat wavelet structure. We extend this idea to lossy compression in Section III-B, where we achieve superior PSNR on the reconstruction of the CFA sampled image. In Section III-C, we detail implementational optimizations. In Section III-D, we further optimize the lossy compression minimizing the error of the reconstructed color image *after* it has undergone the camera processing pipeline.

A. Lossless Compression of CFA sampled images

Recall that $w_{L^*L}^\alpha$ and $w_{L^*L}^\beta$ are scaling coefficients of the same chrominance image α using two conjugate variations of the wavelet transforms. This suggests that the $w_{L^*L}^\alpha$ and $w_{L^*L}^\beta$ are highly correlated, which may decrease coding efficiency. Examining (8) using the LeGall 5/3 wavelet transforms, the plot in Fig. 3(a) demonstrate that $w_{L^*L}^\alpha$ in w_{LH}^y and $w_{L^*L}^\beta$ in w_{HL}^y are highly correlated. Indeed, the strength of correlation by the Pearson product-moment correlation coefficients is 0.9989 [28], [29].

In lossless compression, the coefficients of w_{HL}^y and w_{LH}^y are decorrelated by orthogonal transformation using the sums and differences. To sparsify w_{LH}^y and w_{HL}^y , they are replaced by the decorrelated coefficients v_d^y and v_s^y , as follows:

$$\begin{aligned} v_d^y(\mathbf{n}) &= w_{LH}^y(\mathbf{n}) - w_{HL}^y(\mathbf{n}) \\ &= \left(w_{LH}^\ell(\mathbf{n}) - w_{HL}^\ell(\mathbf{n}) \right) + \left(w_{L^*L}^\alpha(\mathbf{n}) - w_{L^*L}^\beta(\mathbf{n}) \right) \\ v_s^y(\mathbf{n}) &= \left[\frac{1}{2} \left(w_{LH}^y(\mathbf{n}) + w_{HL}^y(\mathbf{n}) \right) \right] \\ &= \left[\frac{1}{2} \left(w_{LH}^\ell(\mathbf{n}) + w_{HL}^\ell(\mathbf{n}) \right) + \frac{1}{2} \left(w_{L^*L}^\alpha(\mathbf{n}) + w_{L^*L}^\beta(\mathbf{n}) \right) \right], \end{aligned} \quad (13)$$

where $\lfloor \cdot \rfloor$ denotes a *floor* operation. Then, w_{HL}^y and w_{LH}^y are perfectly reconstructable from the decorrelated coefficients v_d^y and v_s^y as

$$\begin{aligned} w_{HL}^y(\mathbf{n}) &= v_s^y(\mathbf{n}) - \left\lfloor \frac{v_d^y(\mathbf{n})}{2} \right\rfloor, \\ w_{LH}^y(\mathbf{n}) &= v_d^y(\mathbf{n}) + w_{HL}^y(\mathbf{n}). \end{aligned} \quad (14)$$

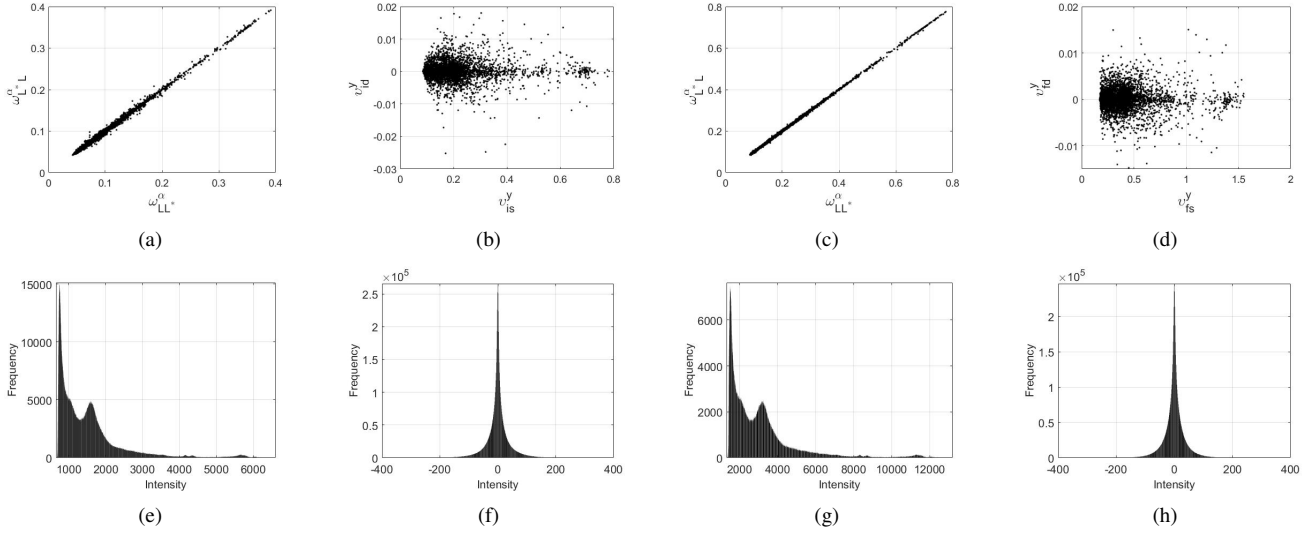


Fig. 3. Illustration of high redundancy in the Mallat wavelet decomposition. (a) Plot of $w_{LL^*}^\alpha$ against $w_{L^*L}^\alpha$ for the LeGall 5/3 wavelet transform. (b) Plot of v_s^y against v_d^y for the LeGall 5/3 wavelet transform. (c) Plot of $w_{LL^*}^\alpha$ against $w_{L^*L}^\alpha$ for the Daubechies 9/7 wavelet transform. (d) Plot of v_s^y against v_d^y for the Daubechies 9/7 wavelet transform. (e) Histogram of $w_{LL^*}^\alpha$ for the LeGall 5/3 wavelet transform. (f) Histogram of $w_{LL^*}^\alpha - w_{L^*L}^\alpha$ for the LeGall 5/3 wavelet transform. (g) Histogram of $w_{LL^*}^\alpha$ for the Daubechies 9/7 wavelet transform. (h) Histogram of $w_{LL^*}^\alpha - w_{L^*L}^\alpha$ for the Daubechies 9/7 wavelet transform.

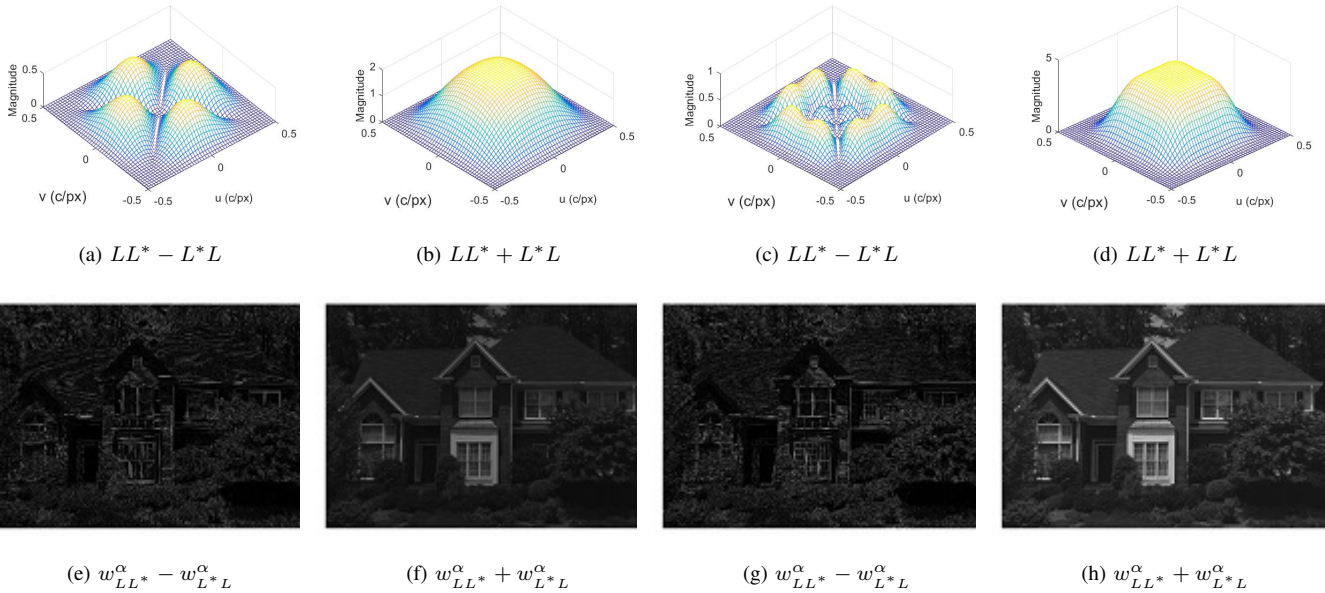


Fig. 4. Filter responses and examples of the filtered coefficients. The spatial frequencies u and v for respectively n_0 and n_1 are normalized in the range -1.0 to 1.0 , where 1.0 corresponds to π radians in cycles per pixel height (c/px [19]). (a), (b), (e), (f) The LeGall 5/3 wavelet transform. (c), (d), (g), (h) The Daubechies 9/7 wavelet transform. The intensity of the filtered coefficients are scaled for display.

The difference subbands v_d^y is designed to decorrelate $w_{LL^*}^\alpha$ and $w_{L^*L}^\alpha$. This is confirmed by Fig. 3(b), and the Pearson product-moment correlation coefficient decreased to -0.0174 . The coding efficiency also increases as demonstrated by the entropy of 6.99 in Fig. 3(f) relative to 11.05 of Fig. 3(e). To understand why this is the case, consider rewriting the difference $w_{LL^*}^\alpha - w_{L^*L}^\alpha$ as the output of a single filtering operation on the signal α by a difference of lowpass filters $LL^* - L^*L$. As evidenced by the frequency responses shown in Fig. 4(a), the difference of lowpass filters forms a bandpass filter, hence suppressing the lowpass signal α . We conclude

that the residual $w_{LL^*}^\alpha - w_{L^*L}^\alpha$ in v_d^y is small (see Fig. 4(e)). Appealing to the fact that v_d^y is dominated by the luminance highpass w_{LH}^ℓ and w_{HL}^ℓ with a very limited contribution from the bandpass chrominance $w_{LL^*}^\alpha - w_{L^*L}^\alpha$, it requires only minimal additional levels (N' in Fig. 5) of wavelet transforms (LeGall 5/3 in our implementation) to sparsify v_d^y . Therefore, we propose to encode v_d^y the same way we would normally encode w_{LH}^ℓ or w_{HL}^ℓ . See Fig. 5.

On the other hand, the sum subband v_s^y is comprised of the lowpass chrominance α and the highpass luminance ℓ . The sum $w_{LL^*}^\alpha + w_{L^*L}^\alpha$ can be thought of as the filtering

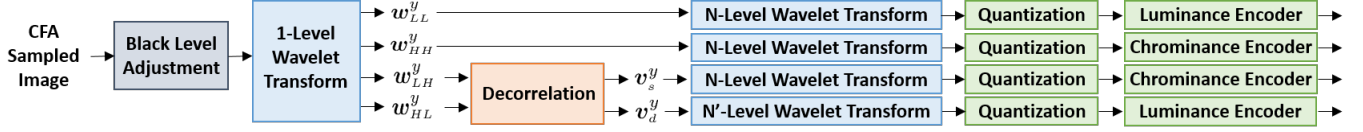


Fig. 5. Description of the proposed compression schemes in Sections III-A and III-B. In lossless compression, the quantization step is not performed.

output of the chrominance signal α through a single filter $LL^* + L^*L$. As shown by the frequency responses in Fig. 4(b) and the filtered images in Fig. 4(f), the sum of lowpass filters $LL^* + L^*L$ also corresponds to a lowpass filter. Hence, the wavelet coefficient v_s^y is a mixture of lowpass chrominance and highpass luminance. We argue that compression should treat v_s^y as we treat the chrominance of w_{LL}^α because the relative magnitudes of the fine scale wavelet coefficients w_{LH}^ℓ and w_{HL}^ℓ are far smaller than the chrominance w_{LL}^α . Hence, we proposed to apply additional N levels of wavelet transforms to v_s^y (where $N > N'$), in a manner similar to the Mallat wavelet packet transform [9]. The Mallat wavelet packet transform coefficients are subsequently encoded by a variable length coding scheme designed for a chrominance component (similar to the way w_{LL}^α would normally be treated). See Fig. 5.

Finally, the wavelet coefficients w_{LL}^y and w_{HH}^y of (8) are interpreted as low frequency components of luminance w_{LL}^ℓ and chrominance $w_{L^*L^*}^\beta$, respectively. Therefore, additional N levels of wavelet transform should be applied to w_{LL}^y and w_{HH}^y , similar in manner to [9]. We apply an encoding scheme of luminance and chrominance to them, respectively. See Fig. 5.

In our compression method, we shift each color component of the CFA sampled image by adjusting its offset before taking wavelet transform, as follows:

$$y'(\mathbf{n}) = y(\mathbf{n}) - \mathbf{c}(\mathbf{n})\mathbf{k} \quad (15)$$

where $\mathbf{k} = [k_r, k_g, k_b]^T$ is the integer offset values of color components (this is commonly performed in camera processing pipelines already). The shift \mathbf{k} must be stored as a sideband information in order to uncompress the image later. In the experiment, the values of \mathbf{k} are chosen by black offset, which was computed from a calibration experiment using X-Rite ColorChecker¹. This has the effect of shifting $v_s^y \simeq (w_{LL^*}^\alpha + w_{L^*L}^\alpha)/2$ and $w_{HH}^y \simeq w_{L^*L^*}^\beta$ toward zero, which increases the coding efficiency further. See Fig. 5.

The image is uncompressed by following the steps in Fig. 5 in the reverse order.

B. Lossy Compression of CFA sampled images

The proposed compression scheme in lossy mode is identical to the lossless scheme in Section III-A as illustrated in Fig. 5, except for the decorrelation step and the quantization step. The wavelet coefficients $w_{LL^*}^\alpha$ in w_{LH}^y and $w_{L^*L}^\alpha$ in w_{HL}^y of the Daubechies 9/7 wavelet transform are also highly correlated, as demonstrated by the strength of the Pearson product-moment correlation coefficient of 0.9989 in Fig. 3(c).

In lossy compression, the w_{LH}^y and w_{HL}^y are decorrelated by a non-integer linear transformation. That is, let

$$\begin{bmatrix} v_s^y(\mathbf{n}) \\ v_d^y(\mathbf{n}) \end{bmatrix} = \mathbf{M} \begin{bmatrix} w_{LH}^y(\mathbf{n}) \\ w_{HL}^y(\mathbf{n}) \end{bmatrix}, \quad (16)$$

where $\mathbf{M} \in \mathbb{R}^{2 \times 2}$. Recalling that we quantize v_s^y and v_d^y (not w_{LH}^y and w_{HL}^y), let $\hat{v}_s^y(\mathbf{n}) = v_s^y(\mathbf{n}) + q_s(\mathbf{n})$ and $\hat{v}_d^y(\mathbf{n}) = v_d^y(\mathbf{n}) + q_d(\mathbf{n})$ denote the quantized versions of v_s^y and v_d^y , respectively, where q_s and q_d are the quantization errors approximated as uniform distribution. By the choice of \mathbf{M} , we minimize the error between the wavelet coefficients w and its quantized coefficients while penalizing non-sparsity of the decorrelated coefficients v , as follows:

$$\begin{aligned} & \arg \min_{\mathbf{M}} \sum_{\mathbf{n}} \left\| \begin{bmatrix} w_{LH}^y(\mathbf{n}) \\ w_{HL}^y(\mathbf{n}) \end{bmatrix} - \mathbf{M}^{-1} \begin{bmatrix} v_s^y(\mathbf{n}) + q_s(\mathbf{n}) \\ v_d^y(\mathbf{n}) + q_d(\mathbf{n}) \end{bmatrix} \right\|_2^2 \\ & \quad + \lambda \sum_{\mathbf{n}} \left\| \begin{bmatrix} v_s^y(\mathbf{n}) \\ v_d^y(\mathbf{n}) \end{bmatrix} \right\|_1 \\ & \simeq \arg \min_{\mathbf{M}} \mathbb{E} \left\{ \sum_{\mathbf{n}} \left(\left\| \mathbf{M}^{-1} \begin{bmatrix} q_s(\mathbf{n}) \\ q_d(\mathbf{n}) \end{bmatrix} \right\|_2^2 + \lambda \left\| \begin{bmatrix} v_s^y(\mathbf{n}) \\ v_d^y(\mathbf{n}) \end{bmatrix} \right\|_1 \right) \right\} \\ & = \arg \min_{\mathbf{M}} \|\mathbf{M}\|_F^2 + \lambda \sum_{\mathbf{n}} \left\| \begin{bmatrix} v_s^y(\mathbf{n}) \\ v_d^y(\mathbf{n}) \end{bmatrix} \right\|_1. \end{aligned} \quad (17)$$

Here, the approximation stems from the law of large numbers (as denoted by the expectation operator $\mathbb{E}\{\cdot\}$) [28], [29] applied to the quantization errors q_s and q_d . The simplification by the Frobenius norm $\|\cdot\|_F^2$ stems from the assumption that q_s and q_d are uniformly distributed and independent. Increasing the value of λ promotes sparsity (and coding efficiency) at the sacrifice of the reconstruction error. In practice, we found that $\mathbf{M} \simeq k \cdot \begin{bmatrix} a & a \\ b & -b \end{bmatrix}$, where the transformation of a and b were stable while k decreased with increasing λ , where $v_s^y \approx ka(w_{LH}^\alpha + w_{HL}^\alpha)$ and $v_d^y \approx kb(w_{LH}^\ell - w_{HL}^\ell)$. We also found that the minimization in (17) can be performed numerically by gradient descent.

The transformation \mathbf{M} decorrelates the coefficients v_s^y and v_d^y as evidenced by the plot of Fig. 3(d) and the Pearson product-moment correlation coefficient decreased to 0.014. The entropy of the decorrelated coefficient reduced to 6.91 of Fig. 3(h) relative to 12.05 of Fig. 3(g).

C. Optimization of Wavelet Transforms

There are two main sources of distortions in lossy compression: round-off error and quantization error. The round-off error stems from finite precision operators used to carry

¹www.xritephoto.com

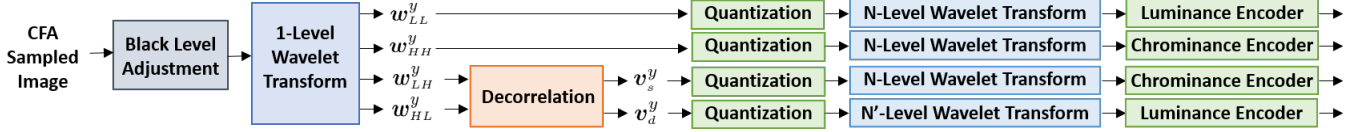


Fig. 6. Description of the ad-hoc alternative lossy compression scheme.

out the forward and reverse wavelet transforms. The quantization error (commonly referred to as the “residual error”) is caused by reducing the number of bits to represent wavelet coefficients, at the expense of accuracy. Specifically, a larger quantization step yields higher compression ratio and higher loss in quality.

The interactions between the two sources of noise depend on the bitrate. Although the quantization errors dominate at the low bitrates, the round-off error limits the image quality at the higher bitrates. This suggests that better quality would be achieved if the round-off error is reduced at the higher bitrates. By experimentation, we heuristically arrived at an alternative decomposition scheme as illustrated in Fig. 6 that perform better at high bitrates. We propose quantizing the coefficients after the first level Daubechies 9/7 wavelet transform and decorrelation step outlined in Section III-B. We then use the LeGall 5/3 to carry out the Mallat wavelet packet transform on w_{LL}^y , w_{HH}^y , and v_s^y . Since LeGall 5/3 transform is reversible, no additional round-off errors are expected (or post-pipeline quarter resolution color image, as described in Section III-D). This is in contrast to the conventional compression scheme of quantizing the coefficients after multiple-level wavelet transform [6].

As the quantization step increases, the round-off error become insignificant relative to the quantization error. Hence at the lower bitrates, we empirically found that Daubechies 9/7 would be more effective for the decorrelated Mallat as described in Section III-B and in Fig. 5. The trade-offs between bitrates and the choice of wavelet transforms are confirmed by our experiments in Section IV-C.

D. Camera Processing Pipeline-Aware Lossy Compression

The decorrelated decomposition schemes in Sections III-A and III-B improve coding efficiency relative to the existing CFA compression schemes. Recalling that the color image is constructed using a decompressed CFA sampled image, there may be additional penalties in image quality when the distortion of the lossy compression is propagated through the camera processing pipeline. Specifically, CFA sampled images are not invariant to the color of illumination, raising the possibility that one color component is potentially compressed more than other components. Similarly, color correction would boost errors in a certain color channel relative to others. The human eyes are more sensitive to the dark regions of the image, which is further exaggerated by gamma correction. Clearly, uniformly quantizing the decorrelated Mallat wavelet packet transform coefficients of the CFA sampled image is suboptimal for minimizing the distortion of the color image we recover from the (decompressed) raw sensor data.

Hence, in this section, we develop a pipeline for compressing CFA sampled images that maximizes the quality of the subsequently reconstructed color images, based on *camera-aware multi-resolution analysis (CAMRA)*. The schematic representation of the proposed pipeline is shown in Fig. 7. Recalling (3), the color components $x(\mathbf{n})$ are reconstructable from ℓ , α , and β by the relation:

$$x(\mathbf{n}) = \begin{bmatrix} 1 & 2 & 1 \\ 1 & 0 & -1 \\ 1 & -2 & 1 \end{bmatrix} \begin{bmatrix} \ell(\mathbf{n}) \\ \alpha(\mathbf{n}) \\ \beta(\mathbf{n}) \end{bmatrix}. \quad (18)$$

Suppose we interpret the $w_{LL}^y \approx w_{LL}^\ell$, $w_{HH}^y \approx w_{LL}^\beta$, and $v_s^y \approx w_{LL}^\alpha$ (or $2kaw_{LL}^\alpha$ if lossy) as the “quarter resolution” versions of ℓ , α , and β . Then by extension of (18) we have the relation

$$w_{LL}^x(\mathbf{n}) \approx \begin{bmatrix} 1 & 2 & 1 \\ 1 & 0 & -1 \\ 1 & -2 & 1 \end{bmatrix} \begin{bmatrix} w_{LL}^y(\mathbf{n}) \\ v_s^y(\mathbf{n}) \\ w_{HH}^y(\mathbf{n}) \end{bmatrix} \quad (19)$$

(replace v_s^y by $v_s^y/2ka$ if lossy). That is, we approximately recover a quarter resolution color image $w_{LL}^x(\mathbf{n})$ directly from the decorrelated one-level wavelet transform coefficients.

We propose to apply color correction, white balance, and gamma correction to the quarter resolution color image w_{LL}^x . See Fig. 7. These steps match the processing that takes place in the digital camera processing pipeline (as described in Section II-C), rendering a quarter resolution version of the final color image $x_{gc,wb,cc}$ that the digital camera would yield (i.e. the image that we are after). See Fig. 8. Hence, we posit that a compression method designed to minimize the distortion of the color corrected, white balanced, gamma corrected low-resolution color image would also maximize the quality of the high-resolution color image subsequently reconstructed from the decompressed CFA sampled image. For instance, Fig. 7 illustrates a subsequent JPEG2000 compression, where we convert the gamma corrected color image to luma/chroma components, perform N -level wavelet transform and quantize before encoding the bits.

Finally, when recovering the quarter resolution color image in (19), a few coefficients can take on negative values. Thresholding them to zero would introduce additional distortion, which is unattractive. Instead, we keep the absolute value of w_{LL}^x , encoding the sign bits separately. The binary image of sign bits is encoded by the standard encoder, which added about 0.004 bits per pixel on average in our tests. The advantages to the compression scheme in Fig. 7 is confirmed by the experiments in Section IV-D.

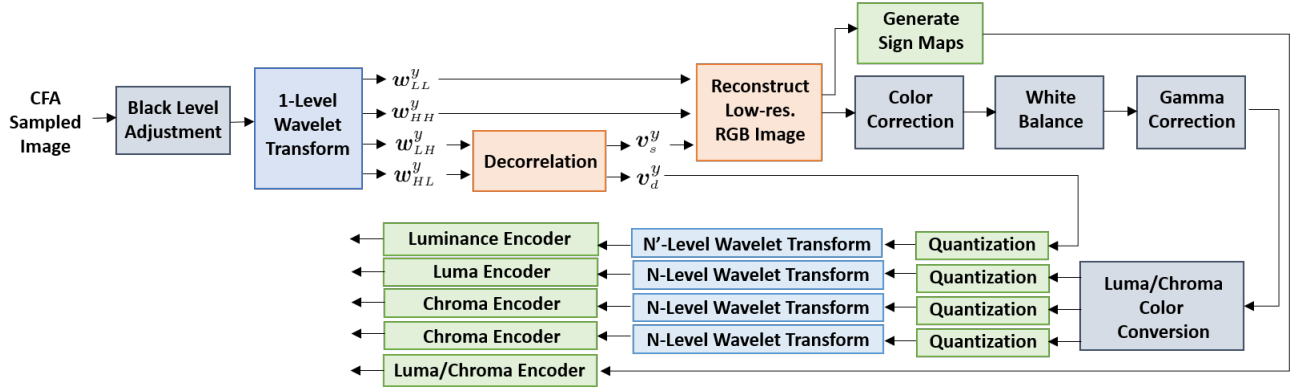


Fig. 7. Description of the proposed compression scheme of CAMRA in Section III-D.



Fig. 8. Comparison of the color image at the end of the pipeline in Section II-C (left) and the quarter resolution color image recovered from the wavelet coefficients in Section III-D (right).

IV. EXPERIMENTAL RESULTS

A. Setup

We verified our proposed method using 64 raw sensor images of Nikon D810 and Sony Alpha a7R II as shown in Fig. 9. These cameras are especially challenging to work with because they lack the optical lowpass filters. (We did not consider the low-resolution Kodak and IMAX images typically used in demosaicking and compression studies, as the resolution of typical modern digital cameras far exceeds them. They also poorly approximate the sensor data, prior to the camera pipeline.) In the proposed method, the transformed images were coded using the standard JPEG2000 codec, *openJPEG*. The level of wavelet transformation was set to 5, which is the default setting of *openJPEG*. The size of a code block was set to 64×64 as a default value. The raw sensor data was cropped to the size 4436×6642 (Nikon) and 4788×7200 (Sony) because of the size limitation of *openJPEG* engine.

For comparison, we decomposed the color images and the raw sensor images using LeGall 5/3 wavelet transform for lossless coding and Daubechies 9/7 wavelet transform for lossy coding of JPEG2000 in different configurations. They are: the wavelet transform on the color images reconstructed in a typical camera processing pipeline (denoted as “RGB” in Table I), the wavelet transform on the CFA sampled images treated as gray images (“CFA”), the wavelet transform on the demultiplexed color images at low resolution (“Demux”), the macropixel spectral-spatial transformation (“MSST”) on

the CFA sampled images [6], and the Mallat wavelet packet transformation on the CFA sampled images (“Mallat”) [9]. see Fig. 10.

B. Lossless Compression of CFA sampled images

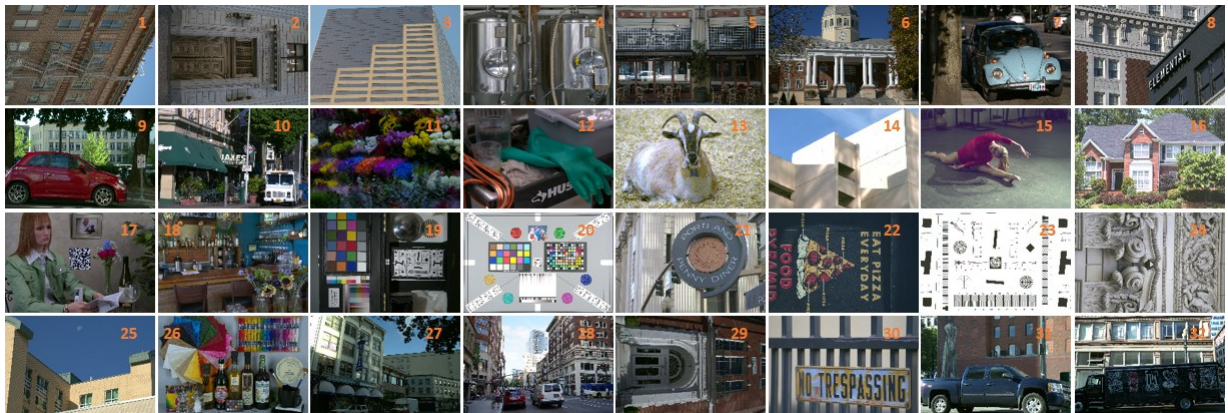
The compression results are tabulated in Table I in terms of bits per pixel (bpp). Our proposed method improves coding efficiency by about 7% (Nikon) and 15% (Sony) relative to the standard JPEG2000 coding. Since the total number of pixel components being coded is three times than that of a CFA sampled image in the standard JPEG2000 coding, the RGB encoding is obviously the least efficient. The large coding gain of Sony camera stems from the fact that the dynamic range of raw data was close to 2^{13} while the processed color image exceeded 2^{13} requiring an extra bit of representation. Typically, the dynamic range of the color images are increased through the camera processing pipeline if raw data are dark, and so this is not entirely unexpected. Relative to directly applying JPEG2000 lossless compression to CFA sampled images, we gained 9.08% (Nikon) and 5.86% (Sony). This can be explained by Fig. 2(b), which shows that the *HL*, *LH*, and *HH* subbands are dominated by non-sparse chrominance components. Relative to the demultiplexing method, the MSST and the Mallat wavelet transform compression schemes improved by about 5% (Nikon) and 0.7% (Sony). The proposed scheme improved further by 0.71% (Nikon) and 0.40% (Sony) relative to the MSST; and 0.36% (Nikon) and 0.41% (Sony) relative to the Mallat wavelet scheme. The bpps in Table I validate our theoretical analysis in Section III that the decorrelated Mallat wavelet packet transform on CFA sampled images reduces bit requirement.

C. Lossy Compression of CFA sampled images

The performance of the proposed decorrelated Mallat packet wavelet scheme in Section III-B and the further optimization scheme in Section III-C were evaluated on the rate-distortion curves in Fig. 11. In the curves, we measured the average peak signal-to-noise ratio (PSNR) of the reconstructed test CFA sampled images, relative to the original CFA sampled images. We applied the standard JPEG2000 lossy coding scheme to the comparing methods (including the method in [9], which was



(a) Test images of Nikon D810



(b) Test images of Sony Alpha a7R II

Fig. 9. Raw sensor images used in our experiments. Source is www.imaging-resource.com, reproduced with a written permission.



Fig. 10. Comparison of one-level decomposition. (a) RGB. (b) CFA. (c) Demux. (d) MSST. (e) Mallat. (f) Proposed.

proposed for lossless coding only). In this experiment, bitrates were controlled by quantization step. We disabled the rate-controller in openJPEG because it confounds the distortion analysis.

The alternative lossy coding scheme in Section III-C outperformed at higher bitrates as predicted in the analysis of Section III. At lower bitrates, the decorrelated Mallat packet wavelet scheme slightly improved the coding efficiency. This demonstrates that round-off error is predominated at higher bitrates, and quantization error increases as bitrates decrease.

D. Lossy Compression with Camera Processing Pipeline

Next, we investigate the effects of distortions introduced by the lossy compression on the camera processing pipeline. For this study, we considered two versions of the camera processing pipeline—one using least square luma-chroma de-

multiplexing (LSLCD) demosaicking [30] and the other using posterior sparsity-directed demosaicking (PSDD) [13].

In Fig. 12, the quality of the color images reconstructed from the decompressed CFA images using digital camera processing pipeline are evaluated in terms of PSNR. For the reference images for PSNR, we applied the same camera processing pipeline to the original CFA image, since it is the best possible image we can obtain without compression.

We report the rate-distortion curves in Fig. 12. The performance of compressing the full RGB image rendered by the camera processing pipeline was better than the existing CFA image compression technique. It suggests that the distortions introduced by lossy compression scheme indeed do propagate through the camera processing pipeline. By contrast, at modest to high bitrate, the proposed camera processing pipeline-aware compression algorithm clearly outperforms the full RGB and the existing CFA image compression schemes.

TABLE I

THE COMPARISON OF BITS PER PIXEL (*bpp*) FOR DIFFERENT DECOMPOSITION METHODS. THE BIT DEPTH OF THE RAW SENSOR READOUT FOR BOTH CAMERAS IS 14 BITS. THE CODING GAIN OF THE PROPOSED METHOD WITH RESPECT TO THE OTHER METHODS IS COMPUTED AS $(bpp \text{ of other methods} - bpp \text{ of our method}) / bpp \text{ of other methods}$ IN PERCENTAGE. THE TOTAL NUMBER OF PIXEL COMPONENTS BEING CODED IS THREE TIMES THAN THAT OF A CFA SAMPLED IMAGE IN THE STANDARD JPEG2000 CODING (*RGB*).

Images	Nikon D810						Sony Alpha a7R II					
	<i>RGB</i>	<i>CFA</i>	<i>Demux</i>	<i>MSST</i>	<i>Mallat</i>	<i>Ours</i>	<i>RGB</i>	<i>CFA</i>	<i>Demux</i>	<i>MSST</i>	<i>Mallat</i>	<i>Ours</i>
1	8.362	8.814	8.605	8.198	8.206	8.204	7.067	6.923	6.496	6.351	6.336	6.296
2	7.186	6.814	6.564	6.187	6.167	6.146	7.461	7.010	6.666	6.591	6.599	6.579
3	7.688	7.894	7.689	7.287	7.264	7.224	7.501	6.816	6.348	6.366	6.359	6.343
4	7.925	7.334	7.142	6.816	6.843	6.842	7.131	6.512	6.127	6.055	6.053	6.035
5	7.714	7.646	7.547	7.132	7.113	7.048	7.144	6.565	6.242	6.157	6.131	6.105
6	7.658	8.037	7.821	7.411	7.384	7.335	7.696	7.177	6.958	6.913	6.882	6.827
7	8.221	8.840	8.476	8.064	8.064	8.048	6.827	6.101	5.755	5.686	5.698	5.668
8	7.949	8.591	8.435	7.970	7.940	7.912	7.098	6.667	6.329	6.242	6.236	6.212
9	7.481	7.440	6.989	6.654	6.662	6.652	7.174	6.150	5.738	5.674	5.718	5.680
10	8.865	8.155	8.050	7.582	7.528	7.499	7.395	6.817	6.563	6.464	6.471	6.429
11	8.278	8.088	7.933	7.530	7.495	7.476	8.937	7.979	7.790	7.802	7.826	7.811
12	9.544	8.841	9.003	8.426	8.329	8.263	6.575	6.222	5.609	5.601	5.618	5.603
13	6.579	8.579	7.735	7.426	7.405	7.390	11.139	8.791	8.598	8.640	8.681	8.690
14	7.594	8.970	8.567	8.196	8.156	8.122	8.006	6.440	6.048	5.995	6.005	5.989
15	7.806	8.106	7.719	7.362	7.349	7.335	7.450	8.189	7.861	7.840	7.824	7.817
16	7.198	7.027	6.847	6.505	6.502	6.474	9.412	7.480	7.482	7.347	7.268	7.205
17	8.583	8.512	8.252	7.872	7.860	7.843	7.241	7.946	7.419	7.387	7.341	7.319
18	10.178	9.180	9.128	8.670	8.650	8.634	8.513	7.344	7.095	7.083	7.103	7.090
19	7.198	7.375	7.245	6.783	6.739	6.699	7.301	6.207	5.987	5.966	5.966	5.944
20	8.000	8.826	8.334	7.937	7.939	7.907	8.272	7.843	7.403	7.434	7.432	7.393
21	6.962	7.676	7.029	6.698	6.709	6.688	7.535	6.820	6.375	6.319	6.333	6.315
22	7.949	8.589	7.638	7.270	7.264	7.277	7.773	6.161	6.087	5.947	5.973	5.931
23	6.733	7.467	7.104	6.683	6.651	6.628	8.183	7.343	6.851	6.850	6.845	6.845
24	7.878	7.721	7.784	7.321	7.229	7.184	8.537	6.937	6.670	6.540	6.537	6.516
25	7.601	7.548	7.485	7.013	6.908	6.871	7.685	6.661	6.181	6.143	6.109	6.093
26	7.327	7.524	7.076	6.752	6.764	6.740	8.024	7.339	7.151	7.073	7.0268	6.988
27	8.203	9.144	8.979	8.461	8.414	8.373	7.241	6.659	6.271	6.296	6.337	6.290
28	7.637	8.119	7.955	7.516	7.471	7.428	7.122	6.762	6.327	6.302	6.376	6.334
29	7.339	7.460	7.218	6.793	6.758	6.734	7.738	6.849	6.533	6.492	6.507	6.470
30	7.422	7.500	7.026	6.658	6.656	6.641	8.274	6.422	6.085	6.073	6.087	6.077
31	10.273	9.403	9.253	8.875	8.809	8.767	7.337	6.829	6.489	6.441	6.403	6.363
32	8.647	7.270	6.951	6.631	6.636	6.624	7.465	6.746	6.430	6.406	6.413	6.380
Average	7.937	8.078	7.800	7.396	7.371	7.344	7.758	6.960	6.624	6.577	6.578	6.551
Our Gain	7.47%	9.08%	5.83%	0.71%	0.36%	—	15.6%	5.86%	1.10%	0.40%	0.41%	—

E. Computational Complexity

The total processing time is dominated by the wavelet transformation and the variable length coding. We only require wavelet transform of a CFA sampled image at the first level, which is one-third the complexity of the JPEG2000 for color images. The decorrelation requires only an addition and a subtraction, which is a negligible overhead. The subsequent N -dimensional wavelet transform is applied three times, comparable to JPEG2000 for color images (after the first level wavelet decomposition); and requires $3/4$ complexity relative to other decomposition schemes in Fig. 10. The number of wavelet coefficients that are encoded by the variable length encoder is one-third of the JPEG2000. Hence, we conclude that the proposed method is substantially less complex than the conventional JPEG2000 and slightly less than other com-

pression schemes.

V. CONCLUSIONS

We proposed a novel lossless and lossy compression schemes for CFA sampled images based on the wavelet analysis of CFA sampling. The analysis proved both theoretically and experimentally that the wavelet coefficients of CFA sampled images are highly correlated. Consequently, we developed the lossless and lossy compression schemes to further sparsify the correlated coefficients. The experimental results verified that the proposed scheme improve coding efficiency relative to the compression of color images. Furthermore, we designed the camera processing pipeline (CAMRA) that minimizes the error of the color images reconstructed from the uncompressed CFA sampled data by the subsequent

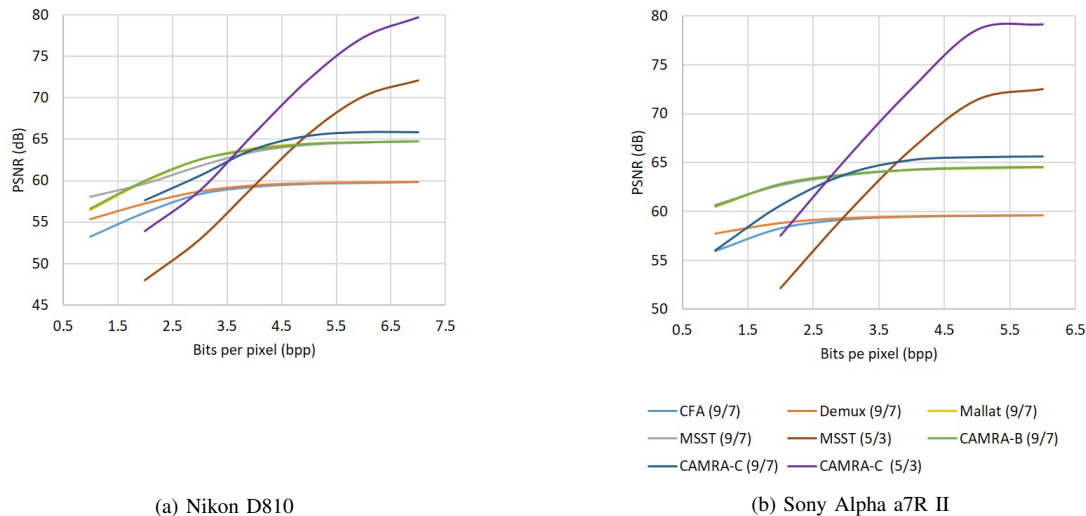


Fig. 11. The comparison of lossy coding schemes. The decorrelated Mallat packet wavelet structure in Section III-B and the further lossy coding scheme in Section III-C are denoted as *Ours* and *Ours-A*, respectively. The Daubechies 9/7 wavelet transform and the LeGall 5/3 were used for the first level in *Ours-A* (9/7) and in *Ours-A* (5/3). The standard coding scheme with MSST decomposition and the lossy coding scheme in [6] are denoted as *MSST* and *MSST-A*.

camera processing pipeline. The experimental results using actual sensor data verified that the proposed decomposition schemes improves coding efficiency relative to the standard color image compression schemes as well as the state-of-the-art compression schemes for CFA sampled images.

REFERENCES

- [1] C.-H. Lin, K.-L. Chung, and C.-W. Yu, "Novel chroma subsampling strategy based on mathematical optimization for compressing mosaic videos with arbitrary rgb color filter arrays in H.264/AVC and HEVC," *IEEE Trans. Circuits Syst. Video Technol.*, vol. 26, no. 9, pp. 1722–1733, Sep. 2016.
- [2] M. Lakshmia, J. Senthilkumarb, and Y. Sureshb, "Visually lossless compression for bayer color filter array using optimized vector quantization," *Applied Soft Comput.*, vol. 46, pp. 1030–1042, Sep. 2016.
- [3] A. Trifan and A. J. R. Neves, "A survey on lossless compression of bayer color filter array images," *Int. J. of Computer, Electrical, Autom., Control and Informat. Eng.*, vol. 10, no. 4, pp. 729–734, Nov. 2016.
- [4] S. Kim and N. Cho, "Lossless compression of color filter array images by hierarchical prediction and context modeling," *IEEE Trans. Circuits Syst. Video Technol.*, vol. 24, no. 6, pp. 1040–1046, 2014.
- [5] D. Lee and K. N. Plataniotis, "A novel high dynamic range image compression scheme of color filter array data for the digital camera pipeline," in *Proc. IEEE Int. Conf. Image Process. (ICIP'12)*, FL, U.S.A., Sep. 2012, pp. 325–328.
- [6] H. S. Malvar and G. J. Sullivan, "Progressive-to-lossless compression of color-filter-array images using macropixel spectral-spatial transformation," in *Proc. IEEE Conf. Data Compression (DCC'12)*, UT, U.S.A., Apr. 2012, pp. 3–12.
- [7] A. A. Moghadam, M. Aghagolzadeh, M. Kumar, and H. Radha, "Compressive demosaicing," in *Proc. IEEE Int. Workshop Multimedia Signal Process. (MMSP'10)*, Saint Malo, France, Oct. 2010, pp. 105–110.
- [8] K.-H. Chung and Y.-H. Chan, "A lossless compression scheme for bayer color filter array images," *IEEE Trans. Image Process.*, vol. 17, no. 2, pp. 134–144, 2008.
- [9] N. Zhang and X. Wu, "Lossless compression of color mosaic images," *IEEE Trans. Image Process.*, vol. 15, no. 6, pp. 1379–1388, 2006.
- [10] S.-Y. Lee and A. Ortega, "A novel approach of image compression in digital cameras with a bayer color filter array," in *Proc. IEEE Int. Conf. Image Process. (ICIP'01)*, Thessaloniki, Greece, Oct. 2001, pp. 482–485.
- [11] C. C. Koh, J. Mukherjee, and S. K. Mitra, "New efficient methods of image compression in digital cameras with color filter array," *IEEE Trans. Consum. Electron.*, vol. 49, no. 4, pp. 1448–1456, 2001.
- [12] K. Hirakawa and P. J. Wolfe, "Rewiring filterbanks for local fourier analysis: Theory and practice," *IEEE Trans. Inf. Theory*, vol. 57, no. 8, pp. 5360–5374, 2011.
- [13] J. T. Korneliussen and K. Hirakawa, "Camera processing with chromatic aberration," *IEEE Trans. Image Process.*, vol. 23, no. 10, pp. 4539–4552, 2014.
- [14] K. Hirakawa, X.-L. Meng, and P. J. Wolfe, "A framework for wavelet-based analysis and processing of color filter array images with applications to denoising and demosaicing," in *Proc. IEEE Int. Conf. Acoust., Speech, Signal Process. (ICASSP'07)*, Hawaii, U.S.A., Apr. 2007, pp. 597–600.
- [15] Y. Lee, K. Hirakawa, and T. Nguyen, "Lossless compression of cfa sampled image using decorrelated mallat wavelet packet decomposition," in *Proc. IEEE Int. Conf. Image Process. (ICIP'17)*, accepted to be published.
- [16] B. E. Bayer, "Color imaging array," U.S. Patent US3971065 A, Jul. 20, 1976.
- [17] B. K. Gunturk, Y. Altunbasak, and R. M. Mersereau, "Color plane interpolation using alternating projections," *IEEE Trans. Image Process.*, vol. 11, no. 9, pp. 997–1013, 2002.
- [18] J. Gu, P. J. Wolfe, and K. Hirakawa, "Filterbank-based universal demosaicking," in *Proc. IEEE Int. Conf. Image Process. (ICIP'10)*, Hong Kong, China, Sep. 2010, pp. 1981–1984.
- [19] E. Dubois, "Frequency-domain methods for demosaicking of bayer-sampled color images," *IEEE Signal Process. Lett.*, vol. 12, no. 12, pp. 847–850, 2005.
- [20] D. Alleysson, S. Susstrunk, and J. Herault, "Linear demosaicing inspired by the human visual system," *IEEE Trans. Image Process.*, vol. 14, no. 4, pp. 439–449, 2005.
- [21] S. Mallat, *A Wavelet Tour of Signal Processing*. San Diego, CA: Academic Press, 1998.
- [22] G. Strang and T. Nguyen, *Wavelets and Filter Banks*. Wellesley, MA: Wellesley-Cambridge Press, 1996.
- [23] A. Choudhury and G. Medioni, "Color constancy using standard deviation of color channels," in *Proc. IEEE Int. Conf. Pattern Recognit. (ICPR'10)*, Istanbul, Turkey, Aug. 2010, pp. 1722–1726.
- [24] G. D. Finlayson, M. S. Drew, and B. V. Funt, "Diagonal transforms suffice for color constancy," in *Proc. IEEE Int. Conf. Comput. Vis. (ICCV'02)*, Berlin, Germany, May 1993, pp. 164–171.
- [25] E. H. Land, "Recent advances in retinex theory and some implications for cortical computations: color vision and the natural image," *Proc. Natl. Acad. Sci. USA*, vol. 80, no. 16, pp. 5163–5169, 1983.
- [26] F. Dufaux, P. L. Callet, R. Mantiuk, and M. Mrak, *High Dynamic Range Video: From Acquisition, to Display and Applications*. San Diego, CA: Academic Press, 2016.
- [27] *Multimedia systems and equipment - Colour measurement and management Part 2-1 Colour management - Default RGB colour space sRGB*, IEC Std. 61966-2-1:1999, 1999.

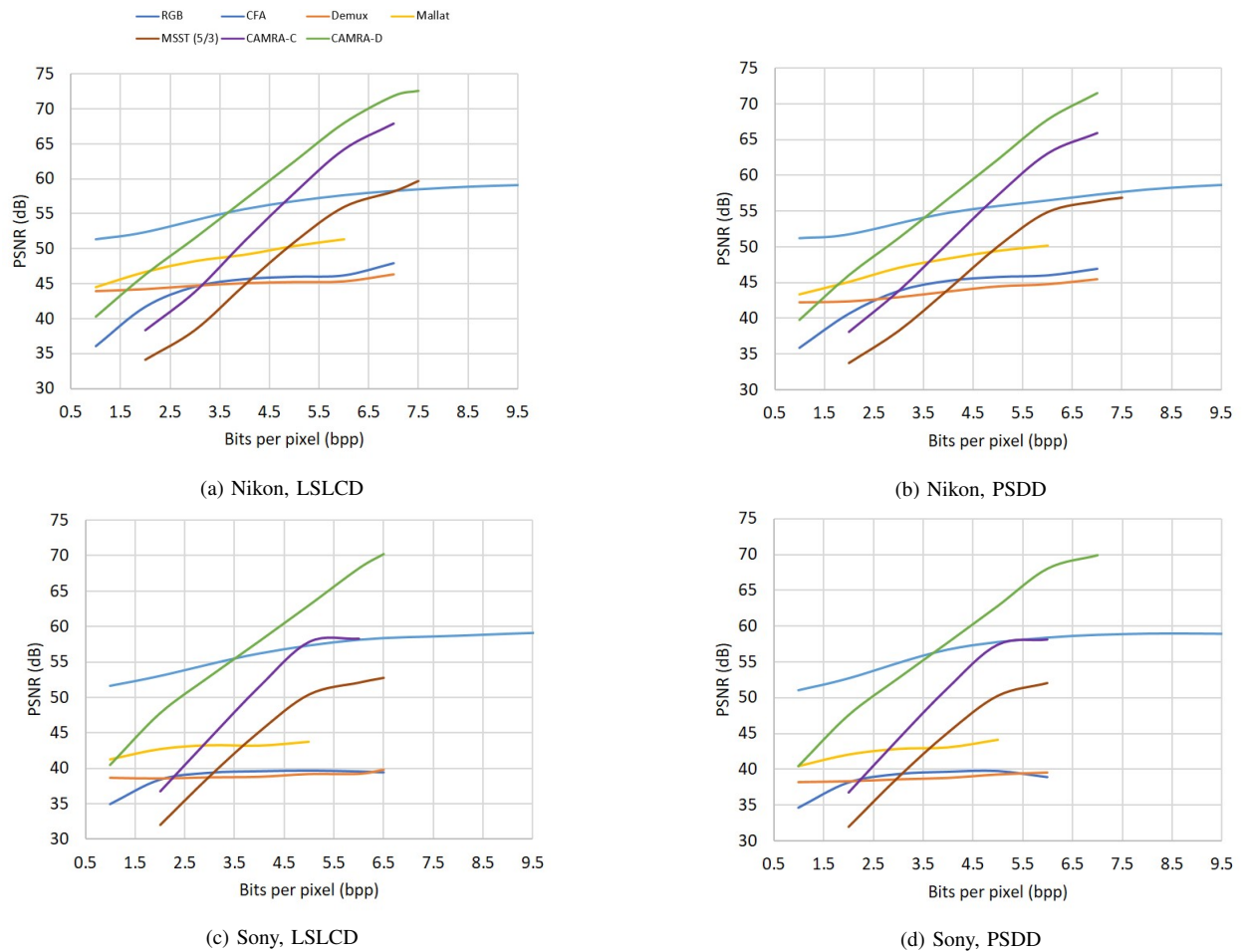


Fig. 12. Performance comparisons of the color images. The pipeline optimization scheme in Section III-D denotes as *Ours-A-P*.

- [28] H. Stark and J. Woods, *Probability, Statistics, and Random Processes for Engineers*. Upper Saddle River, NJ: Pearson, 2011.
- [29] A. Leon-Garcia, *Probability, Statistics, and Random Processes For Electrical Engineering*. Upper Saddle River, NJ: Pearson, 2008.
- [30] G. Jeon and E. Dubois, "Demosaicking of noisy bayer-sampled color images with least-squares luma-chroma demultiplexing and noise level estimation," *IEEE Trans. Image Process.*, vol. 22, no. 1, pp. 146–156, 2013.

ACKNOWLEDGMENT

We thank the staff at Image Resource for giving us the permission to reproduce the raw sensor images used in this study. We also thank openJPEG for the encoding scheme we used to produce results.